Journal of Power Sources 195 (2010) 1333–1343

Contents lists available at ScienceDirect

Journal of Power Sources

journal homepage: www.elsevier.com/locate/jpowsour

Assessment of nickel cermets and $La_{0.8}Sr_{0.2}Sc_{0.2}Mn_{0.8}O_3$ as solid-oxide fuel cell anodes operating on carbon monoxide fuel

Chao Su, Yuzhou Wu, Wei Wang, Yao Zheng, Ran Ran, Zongping Shao*

State Key Laboratory of Materials-Oriented Chemical Engineering, College of Chemistry & Chemical Engineering, Nanjing University of Technology, No. 5 Xin Mofan Road, Nanjing 210009, PR China

ARTICLE INFO

Article history:
Received 15 July 2009
Received in revised form 7 September 2009
Accepted 7 September 2009
Available online 15 September 2009

Keywords:
Solid-oxide fuel cells
Carbon monoxide
Electrochemical performance
Carbon deposition

ABSTRACT

Ni-SDC, Ni-ScSZ, and $La_{0.8}Sr_{0.2}Sc_{0.2}Mn_{0.8}O_3$ (LSSM) anodes are investigated for SOFCs operating on CO. O_2-TPO and SEM results demonstrate LSSM is greatly superior to nickel cermet anodes in suppressing carbon deposition. H_2-TPR suggests there is strong chemical interaction between NiO and ScSZ, which helps to suppress the carbon deposition. Raman spectroscopy of the carbon-deposited nickel cermet anodes demonstrates the graphitization degree of carbon is enhanced with increasing temperature. The cell performance is much lower operating on CO as compared to H_2, and the reduction is the largest for the cell with Ni-SDC anode. Furthermore, steady performance degradation is observed for all three cells operating on pure CO which is irreversible for the cell with Ni-SDC anode while largely reversible for the cell with Ni-ScSZ anode. The degradation for the cell with an LSSM anode is found to be due to the phase instability of LSSM in pure CO atmosphere. By applying a mixture of CO and CO_2 as the fuel or under polarization, the phase of LSSM is stabilized; as a result, the cell is stably operated on CO under current polarization. This suggests that LSSM and Ni-ScSZ anodes are greatly superior to the Ni-SDC anode for operation on CO.

1. Introduction

Nowadays, there is considerable interest in fuel cells for electric power generation because of their high energy efficiency, low emissions, and size flexibility [1]. High-purity hydrogen is generally required as the fuel for polymer-electrolyte-membrane fuel cells with Pt-based electrodes because of their low operating temperature (<100 °C). Concentrations of carbon monoxide that are as low as even 10 ppm in the fuel gas may induce significant degradation of the cell performance [2]. State-of-the-art hydrogen production is mainly from catalytic conversion of hydrocarbons through a series of reactions, including steam reforming, water-shift reaction, and selective oxidation of carbon monoxide in a hydrogen-rich atmosphere (or swing pressure adsorption) [3,4]. Such complicated processes both greatly reduce the operational reliability and decrease the overall fuel efficiency.

Solid-oxide fuel cells (SOFCs) are one important type of fuel cell, which typically operate at 500–1000 °C [5,6]. The elevated operating temperature greatly increases the electrode kinetics, thereby allowing a wide range of chemicals, including hydrocarbons, ammonia, alcohols, and carbon monoxide [7–11], as their potential fuels. Although pure carbon monoxide is seldom directly applied as the fuel because of its high toxicity to human beings, it is one of the most important fuel intermediates in hydrocarbon-fueled SOFCs, direct-carbon fuel cells (DCFCs), and single-chamber solid-oxide fuel cells (SC-SOFCs). Hydrocarbons are believed to be the most promising fuels for SOFCs for near future applications. Although there is increasing interest in direct electrochemical oxidation of hydrocarbons over the anode [12–14], to reduce the coke formation from thermal or catalytic cracking of the hydrocarbons and to increase the power output, these fuels have been more frequently converted into a mixture of hydrogen, carbon monoxide, water, and carbon dioxide by steam reforming, partial oxidation, or autothermal reforming, both externally and internally [15–19]. On the other hand, direct-carbon fuel cells (DCFCs) have attracted increasing attention recently due to their high energy conversion efficiency and wide availability of carbon resources [20,21]. In the DCFCs, carbon monoxide plays an important role in the electrochemical oxidation of solid carbon through the reverse Boudouard reaction: $C + CO_2 = 2CO$ [22,23]. Nowadays, there is increasing interest in SC-SOFCs for mobile applications because of their sealant-free feature and capability for quick startup and shutdown. The successful operation of SC-SOFCs strongly relies on the partial oxidation of fuel to syngas (a mixture of $CO + H_2$) over the anode [24–28]. Therefore, the performance of the hydrocarbon-fueled SOFCs, DCFCs, and SC-SOFCs is closely related with the carbon monoxide oxidation over the anode. An investigation of SOFCs operating on carbon monoxide fuel has great practical importance.

* Corresponding author. Tel.: +86 25 83172256; fax: +86 25 83172256.
E-mail address: shaozp@njut.edu.cn (Z. Shao).

0378-7753/$ – see front matter © 2009 Elsevier B.V. All rights reserved.
doi:10.1016/j.jpowsour.2009.09.015

Compared to the vast amount of research on hydrogen fuel, carbon monoxide as a fuel of SOFCs has been much less investigated. To date, few publications have been available regarding SOFCs operating on carbon monoxide or CO-containing fuels [11,29–36]. Similar to other carbon-containing fuels, one difficulty associated with carbon monoxide fuel may be carbon deposition over the anode surface, since the Boudouard reaction, $2CO = CO_2 + C$, is favored at the operating temperatures of SOFCs. To achieve a stable cell performance, the carbon deposition over the anode should be suppressed. Although thermodynamic calculation can be applied to predict the propensity of coke formation, the reaction kinetics may be more important in a real operating fuel cell. The effect of current density, operating temperature, and the other gas components, such as hydrogen and water, on the carbon deposition over nickel cermet anode, typically Ni-YSZ anode, has been experimentally investigated by different researchers [11,29–36].

In this study, the effect of anode composition on the carbon deposition, the cell performance, and performance degradation was investigated. A comparative study of Ni-$Sm_{0.2}Ce_{0.8}O_{1.9}$ (SDC) and Ni-$(Sc_2O_3)_{0.1}(ZrO_2)_{0.9}$ (ScSZ) cermet anodes and a $La_{0.8}Sr_{0.2}Sc_{0.2}Mn_{0.8}O_3$ (LSSM) perovskite-type oxide anode is presented.

2. Experimental

2.1. Synthesis and fabrication

SDC, ScSZ, LSSM, $Ba_{0.5}Sr_{0.5}Co_{0.8}Fe_{0.2}O_{3-\delta}$ (BSCF), and $La_{0.8}Sr_{0.2}MnO_3$ (LSM) oxide powders were all synthesized by an EDTA–citrate complexing sol–gel process [37]. Their firing temperatures were 800, 900, 1000, 950, and 950 °C, respectively. Fuel cells with anode-supported thin-film electrolyte configuration were adopted for the evaluation of the performance of Ni-SDC and Ni-ScSZ anodes, while fuel cells with electrolyte-supported configuration were selected for the LSSM anode due to the fabrication difficulty for LSSM-supported cells. Anode-electrolyte dual-layer cells were fabricated by dual dry pressing/high temperature sintering. Anode powders, composed of 55.8 wt.% NiO, 37.2 wt.% SDC (or ScSZ), and 7.0 wt.% polyvinylpyrrolidone (PVP) as a pore former, were well mixed in liquid ethanol by ball milling at 30 rpm for 24 h. The mixture was then dried at 80 °C and sieved to 200 mesh. To prepare the anode-electrolyte dual-layer cells, the anode powder was first pressed into disk-shaped anode substrate (15 mm in diameter) at 120 MPa. A proper amount of SDC (or ScSZ) powder was then distributed homogeneously over the anode surface and pressed again at 240 MPa. The green cells were then calcined at 1400 °C (or 1500 °C for ScSZ electrolyte) to sinter the electrolyte layer. Next, the cathode slurries were sprayed over the electrolyte surface in a round shape using a modified spraying gun (BD-128, Fenghua Bida Machinery Manufacture Co. Ltd., Fenghua, China), and the temperature of cells was kept at ~220 °C by a hot plate. Air was used as the carrier gas at a working pressure of 1 atm. In the spray process, the distance between the spraying gun and the cells was 15 mm, and the spray time was ~20 min. Then the cells were fired at 1000 °C for 2 h for the BSCF electrode (or 1100 °C for LSM). The effective geometric surface area is typically ~0.48 cm^2. To prepare the electrolyte-supported cells, dense ScSZ pellets (>97% of theoretical density) were obtained by uniaxially pressing powders into disks at 240 MPa for 2 min (diameter of 15 mm) and sintered at 1500 °C for 5 h. Both faces of the ScSZ pellets were then polished to reduce the membrane thickness to ~0.2 mm. LSSM cathode and LSSM anode were spray-deposited onto the electrolyte surfaces and fired at 1150 °C for 2 h. The effective electrode surface area is 0.26 cm^2. Silver and gold were selected as the current collectors for the cathode and anode, respectively.

2.2. Basic characterization

The phase structure of the samples was examined by an X-ray diffractometer (XRD, ARL X' TRA) equipped with Cu Kα radiation (λ = 0.1541 nm). The scans were performed in the 2θ range 20–80°. The surface morphologies of the fuel cells were examined by using an environmental scanning electron microscope (ESEM, Quanta-2000).

Hydrogen temperature-programmed reduction (H_2-TPR) was performed to identify the interaction of NiO with the ceramic component (ScSZ or SDC). Approximately 0.03 g sample was placed into a U-type quartz reactor with an inner diameter of ~4 mm. The sample was pretreated under pure argon atmosphere at the flow rate of 30 ml min^{-1} at room temperature for 30 min to get rid of any weakly adsorbed surface species. The atmosphere was then switched to 10 vol.% H_2–Ar. After stabilization of the baseline, the reactor was programmatically heated to 930 °C at 10 °C min^{-1}; the consumption of hydrogen was monitored by an in situ TCD detector using a BELCAT-A apparatus.

For carbon deposition tests, about 0.1 g anode powder (Ni-SDC, Ni-ScSZ, or LSSM) was first placed into a U-type quartz reactor (ID: 4 mm) and treated at various temperatures (600, 850, and 900 °C) under a pure carbon monoxide atmosphere at the flow rate of 60 ml min^{-1} for 5 h. The sample was then cooled down to room temperature under a carbon monoxide atmosphere. Approximately 0.01 g anode powder from the treatment was placed into a new U-type quartz reactor with an inner diameter of ~4 mm. 10 vol.% O_2–Ar at the flow rate of 15 ml min^{-1} [STP] was then introduced into the reactor. After flowing with the gas at room temperature for 30 min, the reactor was programmatically heated to 930 °C at 10 °C min^{-1}. The deposited solid carbon over the catalyst surface was then progressively oxidized into gaseous CO_2. This process is called oxygen temperature-programmed oxidation (O_2-TPO). The effluent gas from the reactor was connected with a Hiden QIC-20 Mass spectrometer (MS) for in situ monitoring of the concentration variation of CO_2. At times, the CO_2 desorption was not completed at 930 °C; the furnace temperature was then maintained at 930 °C until the CO_2 signal returned to the baseline.

The laser Raman spectroscopy of the Ni-SDC, Ni-ScSZ, and LSSM anodes after the treatment at various temperatures (600, 850, and 900 °C) under a pure CO atmosphere for 5 h was obtained in an HR800 UV Raman microspectrometer (JOBIN YVON, France) using the green line of an argon laser (λ = 514.53 nm) as excitation source.

2.3. Electrochemical characterization

The *I–V* polarization of the cells was measured using a Keithley 2420 source meter based on the four-probe configuration. During the measurement, carbon monoxide or 3% water humidified hydrogen as the fuel was fed into the anode chamber at a flow rate of 60 ml min^{-1} [STP] while ambient air was the cathode atmosphere. The electrode performance was investigated with a complete cell configuration by the AC impedance method using an electrochemical workstation composed of a Solartron 1287 potentiostat in combination with a 1260A frequency response analyzer. The applied frequency ranged from 0.1 Hz to 100 kHz with signal amplitude of 10 mV under open circuit voltage (OCV) conditions. The LSSM anode was also investigated by current polarization based on the three-electrode configuration by using a Solartron 1287 potentiostat.

3. Results and discussion

3.1. Basic properties

Fig. 1 shows the room-temperature X-ray diffraction patterns of the three anodes, NiO-SDC composite, NiO-ScSZ composite, and

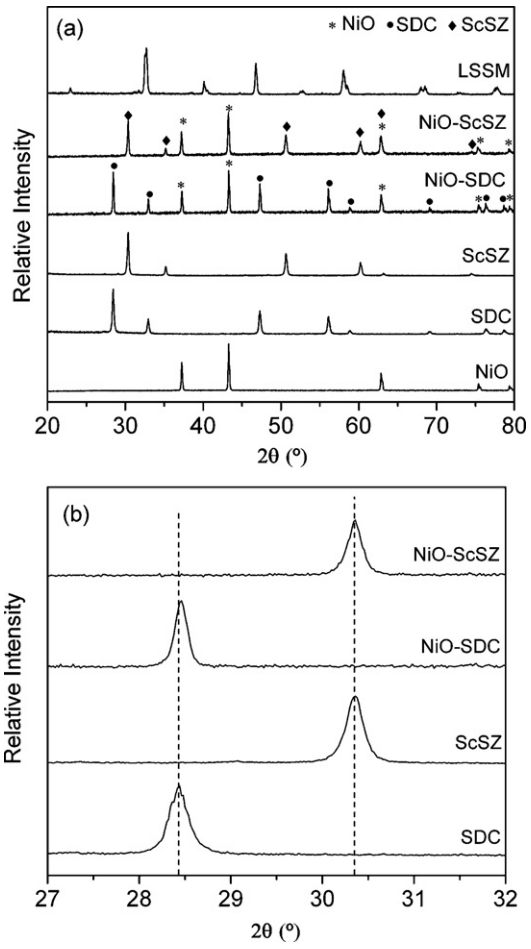

Fig. 1. XRD patterns of NiO, SDC, ScSZ, NiO-SDC, NiO-ScSZ, and LSSM (a), and a magnification of the diffraction peaks of SDC, NiO-SDC, ScSZ, and NiO-ScSZ Bragg 2θ between 27° and 32° (b).

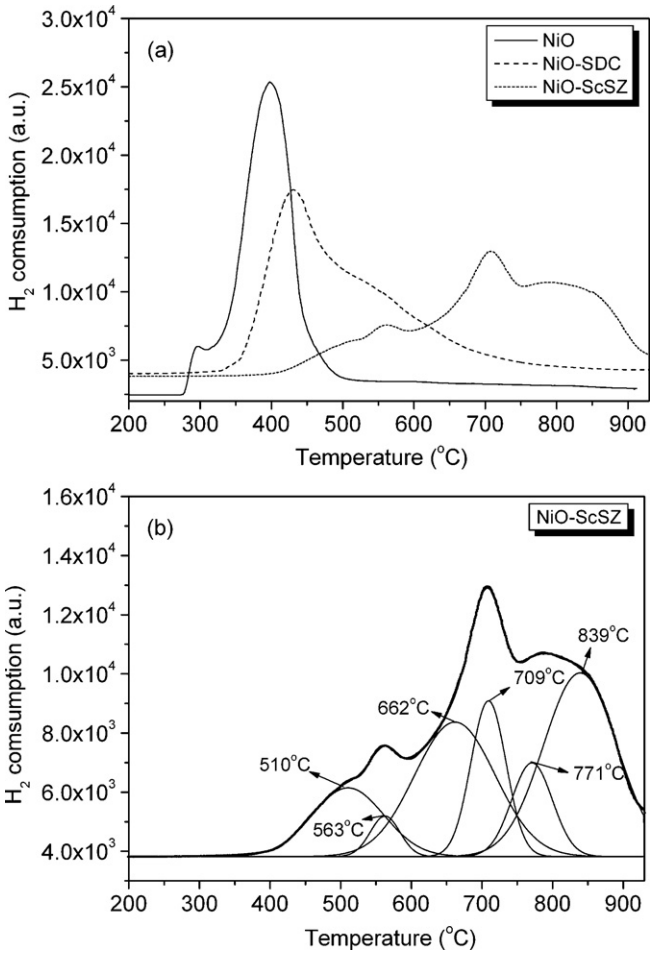

Fig. 2. H_2-TPR profiles of NiO, NiO-SDC, and NiO-ScSZ (a), and fitted results of Ni-ScSZ (b).

LSSM, after calcination at 1400, 1500, and 1150 °C for 5 h (or 2 h for LSSM), respectively; for comparison, the XRD patterns of phase-pure NiO, SDC, and ScSZ are also presented. The diffraction peaks of LSSM can be indexed well based on a perovskite structure with an orthorhombic symmetry, with space group $R\bar{3}c$, and cell parameters of $a = 7.900(0)$ Å, $b = 5.536(2)$ Å, and $c = 5.497(5)$ Å, agreeing well with our previous report [38]. For both nickel cermet anodes, all of their Brag diffraction peaks can be perfectly indexed based on a physical mixture of NiO and SDC or NiO and ScSZ. Fig. 1b shows a magnification of the diffraction peaks of the SDC at miller index (1 1 0) and of the ScSZ at miller index (1 1 0). The diffraction peaks of the SDC phases matched fairly well with each other, as did the diffraction peaks of the ScSZ phases. The lattice parameter is closely related with the ionic radius of the dopant. The ionic radii of Ni^{2+}, Ce^{4+}, and Zr^{4+} (in six coordinations with O^{2-}) are 0.69, 0.87, and 0.72 Å, respectively. This suggests that the incorporation of nickel into SDC should result in the shrinkage of the lattice parameter. In other words, the shift of the diffraction peaks to the higher angle is expected because of the much smaller ionic radius of Ni^{2+} than of Ce^{4+}. However, no obvious peak shift was actually observed. This suggests that no significant phase reaction occurred between NiO and SDC in the NiO-SDC anode, even after sintering at 1400 °C. Regarding NiO-ScSZ, due to the similar ionic size of Ni^{2+} and Zr^{4+}, it is not possible to get the phase reaction information solely based on the peak shift.

The interaction of nickel catalyst with the substrate may have a significant impact on its catalytic activity and its resistance to coke formation when operating on hydrocarbon fuels [39]. To further exploit the possible interaction between NiO and the ceramic component (SDC or ScSZ) in the nickel cermet anodes, H_2-TPR of the NiO-SDC and NiO-ScSZ anodes was conducted, with the results shown in Fig. 2; for comparison, the H_2-TPR profile of pure NiO is also presented. For the nickel oxide sintered at 1400 °C, the reduction started at around 275 °C, peaked at around 400 °C, and completed at around 500 °C. For the NiO-SDC anode, the reduction started at around 330 °C, peaked at around 440 °C, and finished at around 800 °C. The reduction temperature of NiO-SDC, which is only slightly higher than that of the single-phase NiO, suggests that the interaction between NiO and SDC is weak in the NiO-SDC anode, agreeing well with the XRD results. The slightly higher reduction temperature of the NiO-SDC cermet anode than that of the pure NiO could be attributed to the blocking effect of the SDC phase for the free gas diffusion in the NiO-SDC cermet.

Regarding NiO-ScSZ cermet anode, very different hydrogen reduction behavior was observed. As shown in Fig. 2b, the reduction curves are more complicated and less symmetric. This suggests more complex nickel environments in the NiO-ScSZ anode. By numerous simulations, the H_2-TPR curve can be separated into six successive reduction peaks, with the peak temperatures of 510, 563, 662, 709, 771, and 839 °C. This suggests that there may be six different types of nickel oxide environments in the NiO-ScSZ cermet anode. Considerable amount of the NiO had a certain type of interaction with the ScSZ ionic conducting phase. Higher peak temperatures indicate stronger interactions between NiO and ScSZ. The

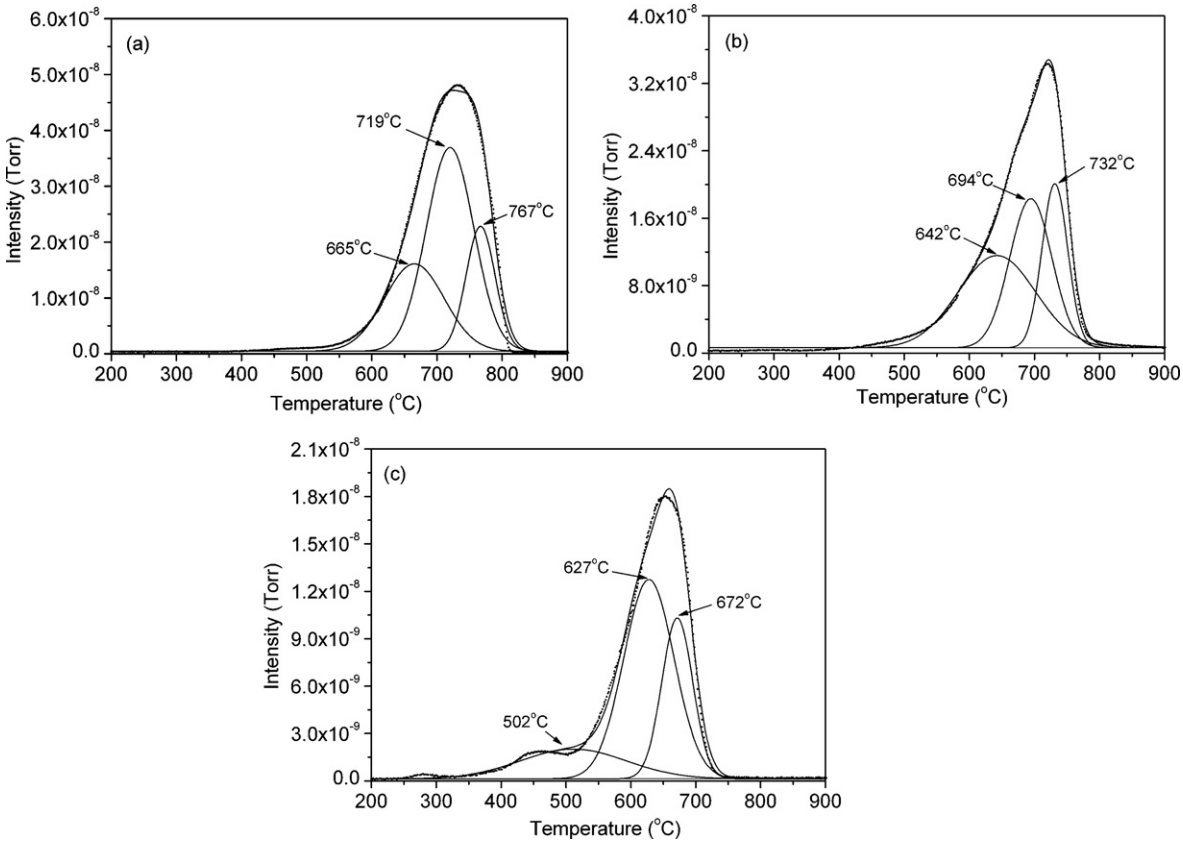

Fig. 3. O_2-TPO profiles and fitted results of the Ni-SDC anode after treatment in pure CO for 5 h at 900 °C (a), 850 °C (b), and 600 °C (c).

effect of the interaction of nickel with ScSZ in the Ni-ScSZ anode on the coke formation properties will be discussed later.

3.2. Carbon deposition

The Boudouard reaction $2CO = C + CO_2$ is thermodynamically favored at the operating temperatures of SOFCs, i.e., 500–1000 °C. Therefore, carbon deposition over the fuel cell anode is a big concern when operating on CO fuel. The coke formation properties of the three anodes under CO atmosphere were first investigated by exposing the anode materials to a pure CO atmosphere at various temperatures (600, 850, and 900 °C) for a fixed period of 5 h, followed by rapid cooling to room temperature under CO, and analysis by O_2-TPO. Fig. 3 shows the O_2-TPO profiles of the various carbon-deposited Ni-SDC anodes. Considerable amount of CO_2 was released during the O_2-TPO process. This suggests that significant carbon deposition over the Ni-SDC anode occurred after exposure to the CO atmosphere. The O_2-TPO curves can be reduced to three successive peaks, with the peak temperatures listed in Table 1. The increase of the treatment temperature resulted in increasing CO_2 peak intensity and a shift of the CO_2 peaks to higher temperatures. Thermodynamically, the Boudouard reaction should be more favored at lower temperature, i.e., the theoretical amount of carbon formation is 0.1175, 0.1575 and 0.4355 molC (molCO)$^{-1}$ at 900, 850, 600 °C, respectively. The larger amount of CO_2 released during the O_2-TPO process at higher treatment temperature suggests that the kinetics played a more important role than did the thermodynamics in the carbon deposition over the Ni-SDC anode. The shift of the CO_2 peak to the higher temperature with increasing treatment temperature indicates the increasing difficulty in eliminating such deposited carbon.

As compared to Ni-SDC, the CO_2 peak intensity for the Ni-ScSZ anode is much weaker, and the carbon formation rate over the Ni-ScSZ anode is less than 1/3 of that over the Ni-SDC anode at the corresponding temperature (Table 2). This suggests that Ni-ScSZ is superior to Ni-SDC in suppressing the carbon formation when operating on CO fuel. In literature, it has also been reported that Ni-ScSZ anode had better resistance towards carbon deposition than Ni-SDC when exposed to propane fuel [19]. In connection with the H_2-TPR results, the stronger interaction between the nickel and the ceramic component suppressed the coke formation over the Ni-ScSZ anode. Similarly to their H_2-TPR profiles, the O_2-TPO curves

Table 1
The peak temperatures of O_2-TPO fitted profiles of Ni-SDC and Ni-ScSZ anodes after the treatment in pure CO for 5 h, at 900, 850 and 600 °C.

Sample	Temperature (°C)	Peak temperature (°C)		
Ni-SDC	900	665	719	767
	850	642	694	732
	600	502	627	672
Ni-ScSZ	900	761	856	883
	850	650	704	806
	600	499	617	754

Table 2
The formation rate of carbon of Ni-SDC and Ni-ScSZ anodes in a pure CO atmosphere for 5 h, at 900, 850 and 600 °C.

Sample	Temperature (°C)	Formation rate of carbon (gC (gNi min)$^{-1}$)
Ni-SDC	900	8.87×10^{-4}
	850	5.54×10^{-4}
	600	2.68×10^{-4}
Ni-ScSZ	900	2.70×10^{-4}
	850	1.55×10^{-4}
	600	2.01×10^{-5}

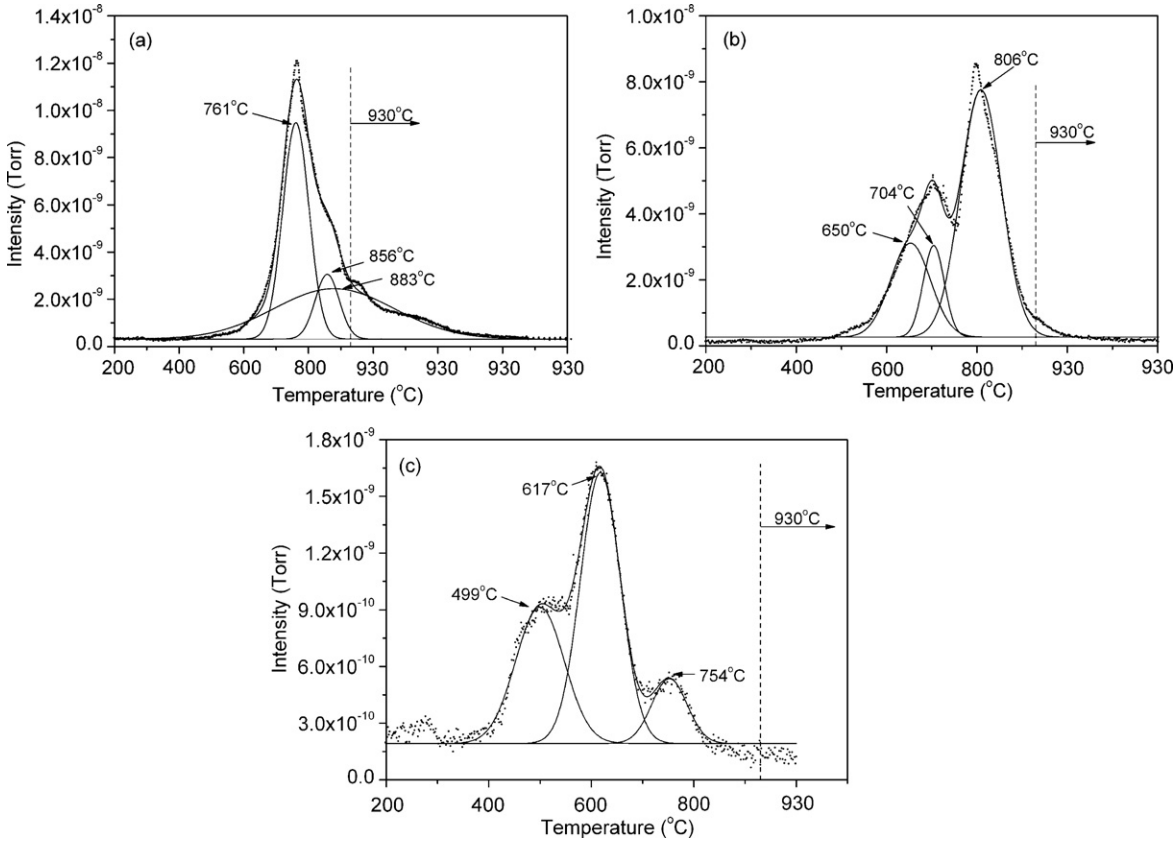

Fig. 4. O_2-TPO profiles and fitted results of Ni-ScSZ anode after treatment in pure CO for 5 h, at 900 °C (a), 850 °C (b), and 600 °C (c).

of Ni-ScSZ are more complicated and less symmetric than those of Ni-SDC. As shown in Fig. 4, they can also be split into three peaks, with the peak temperatures listed in Table 1. As compared to Ni-SDC, the corresponding peak temperature is higher for Ni-ScSZ. This suggests that the carbon deposited over Ni-ScSZ is harder to be eliminated than that in Ni-SDC.

In dramatic contrast from the nickel cermet anodes, there was almost no carbon deposition over the LSSM surface after exposure to CO. As shown in Fig. 5, the CO_2 peak intensity is very weak after exposure to the pure CO atmosphere at various temperatures for 5 h. This suggests high resistance of the LSSM anode towards coke formation when operating on CO fuel. The excellent resistance of perovskite oxide towards carbon deposition has also been reported by other groups [40,41].

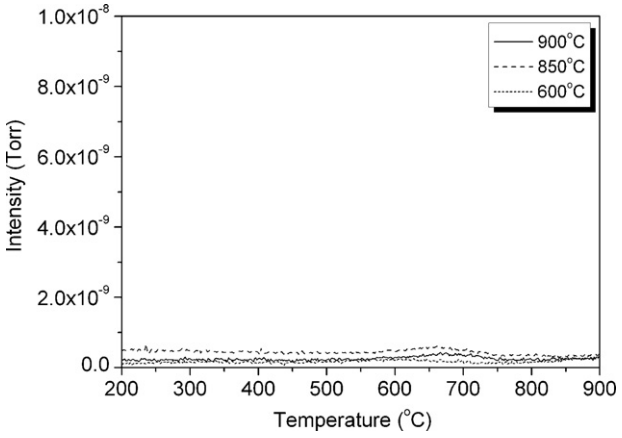

Fig. 5. O_2-TPO profiles of LSSM anode after treatment in pure CO for 5 h at various temperatures.

To investigate the type of the deposited carbon over nickel-based anodes, the laser Raman spectroscopy of the carbon-deposited Ni-SDC, Ni-ScSZ and LSSM samples was measured. As shown in Fig. 6a and b, there are two main bands (D and G) in the first-order Raman spectrum of carbon materials. The D band (~1360 cm^{-1}) and the G band (~1580 cm^{-1}) represent the amorphous structure and the graphite structure, respectively. The degree of structural order of the carbon can be characterized by Raman spectral parameters, such as the full-widths at half maximum (FWHM) of D and G bands and the integrated intensity ratio in the form of $R(I_D/I_G)$ [42,43], which are all listed in Table 3. We know from literature that the value of R decreases with increasing degree of order of the carbon [43,44]. In fact, we also find that the FWHM of D and G bands and the value of R decrease with increasing treating temperature. This clearly shows that the values of R of the carbon deposited over Ni-SDC and Ni-ScSZ anode at 900 °C are only 0.31 and 0.22, respectively. This indicates that the carbon deposited at higher temperatures is almost graphite structure and difficult to eliminate. As shown in Fig. 6c, there is no band detected in the first-order Raman spectrum of carbon materials for the LSSM anode. The results are in good agreement with the O_2-TPO results.

Table 3
Raman spectral parameters of the deposited carbon over nickel-based anodes.

Sample	Temperature (°C)	FWHM (cm^{-1})		$R(I_D/I_G)$
		D-band	G-band	
Ni-SDC	600	61.44	64.87	0.87
	850	51.12	33.94	0.51
	900	41.89	20.20	0.31
Ni-ScSZ	600	52.40	60.93	0.92
	850	45.53	25.12	0.48
	900	38.66	18.25	0.22

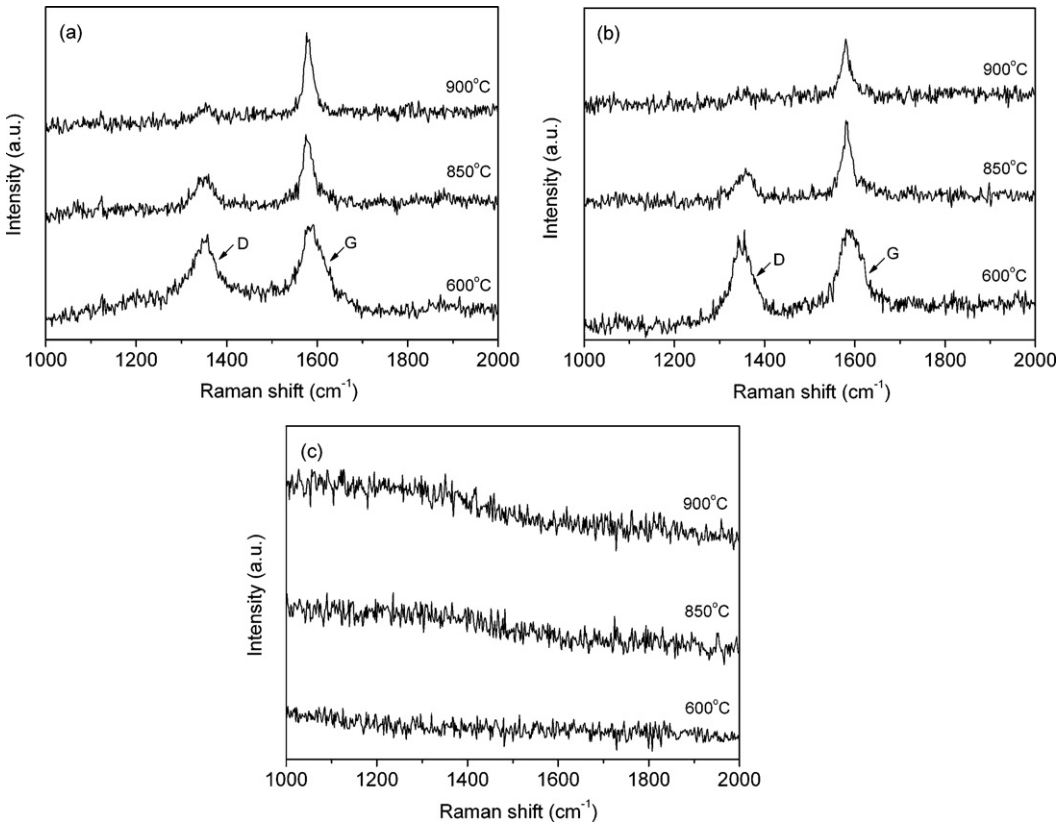

Fig. 6. Raman spectra of Ni-SDC anode (a), Ni-ScSZ anode (b), and LSSM anode (c) after treatment in pure CO for 5 h at various temperature.

To further explore the coke formation over the anodes, Ni-SDC, Ni-ScSZ, and LSSM anodes were flowed with CO atmosphere at the flow rate of 60 ml min^{-1} under OCV conditions at 600, 850, and 900 °C for 5 h, and then subjected to SEM examinations, with the results shown in Fig. 7. For comparison, the SEM morphologies of fresh Ni-SDC and Ni-ScSZ anodes (pre-reduced by hydrogen) and the LSSM anode are also presented. There was obvious carbon deposition which is spherical in shape over the Ni-SDC electrode surface. For the Ni-ScSZ electrode, much less carbon was detected, which is in a flake shape. For the LSSM anode, no carbon was detected by the SEM. The results are in good agreement with the O_2-TPO results.

3.3. Cell performance

To demonstrate the performance of Ni-SDC, Ni-ScSZ, and LSSM anodes operating on CO fuel in real fuel cells, single cells with the composition of Ni-SDC|SDC (20 μm)|BSCF, Ni-ScSZ|ScSZ (20 μm)|LSM, and LSSM|ScSZ (200 μm)|LSSM were fabricated. Fig. 8 shows the *I–V* curves and the corresponding EIS under OCV conditions of the cell Ni-SDC|SDC|BSCF operating on pure CO fuel. For comparison, the *I–V* curves operating on 3% water humidified hydrogen fuel are also presented. A peak power density (PPD) of ~1000 mW cm^{-2} was achieved at 600 °C when operating on hydrogen fuel. Such performances are similar to previous reports [45–47]. As shown in Fig. 8b, the PPD is much smaller when the fuel was changed from H_2 to CO. It reduced to only ~180 mW cm^{-2} at 600 °C, suggesting that the electrochemical activity of CO is much lower than H_2. Indeed, it was reported that the CO oxidation reaction over the Ni-YSZ anode in the active state is more than one order of magnitude slower than the hydrogen oxidation reaction [30]. The much slower electrode kinetics for the CO electro-oxidation than that of the hydrogen over the Ni-SDC anode was further supported by the EIS results, as shown in Fig. 8c and d. The ASR was determined from the impedance spectra, where high-frequency offset is due primary to the electrolyte resistance, while the difference between the high and low frequency intercepts on the real axis (Z') is associated with the electrode contribution, here including both the anode and the cathode. Since the same cell was adopted for operating on H_2 and CO fuels, the difference between the electrode polarization resistances operating on H_2 and CO fuels is originated from the anode. As shown in Fig. 8c, when H_2 was the fuel, the electrolyte resistance (~0.14 Ω cm^2) overwhelmed the electrode polarization resistance (~0.05 Ω cm^2) even at 550 °C. However, the electrode polarization resistance obviously increased when the fuel was changed from H_2 to CO. For example, at 550 °C, the electrode polarizations were 0.05 and 0.4 Ω cm^2, operating on H_2 and CO, respectively.

Fig. 9 shows the cell performances of Ni-ScSZ|ScSZ|LSM operating on H_2 and CO fuels between 750 and 850 °C. When hydrogen was the fuel, a peak power density of ~500 mW cm^{-2} was achieved at 850 °C, which is comparable to our previous reports [48]. When CO was the fuel, the PPD still reached approximately 260 mW cm^{-2}. The difference in power outputs for the cell Ni-ScSZ|ScSZ|LSM operating on H_2 and CO fuels is much smaller than that for the cell Ni-SDC|SDC|BSCF. This could be explained by the increased reaction kinetics of the CO electrochemical oxidation over the nickel cermet anode because of the higher operating temperature.

When LSSM was adopted as the anode, the cell also delivered promising cell performance. As shown in Fig. 10, peak power densities of ~170 and 120 mW cm^{-2} were achieved at 900 and 850 °C, respectively, when operating on hydrogen fuel, while they were approximately 110 and 80 mW cm^{-2}, respectively, operating on CO fuel. This indicates that LSSM is a potential anode material of SOFCs for operating on CO fuel. The relatively lower cell performance as compared to other two cells is due to its much thicker electrolyte.

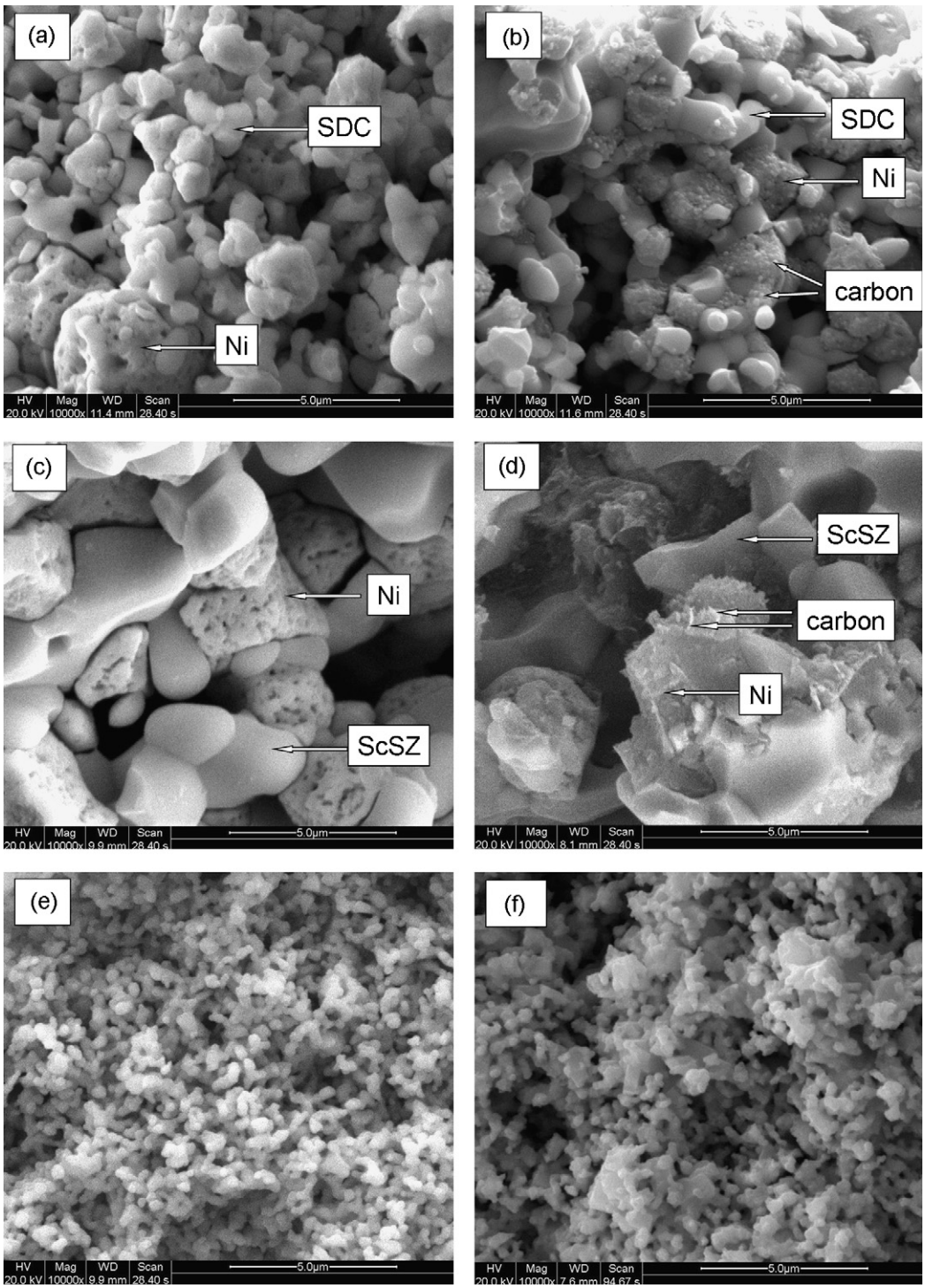

Fig. 7. SEM photos of the cross-sectional views of the cell Ni-SDC|SDC|BSCF reduced by H_2 (a), after operation with pure CO at 600 °C for 5 h under open circuit conditions (b), the cell Ni-ScSZ|ScSZ|LSM reduced by H_2 (c), after operation with pure CO at 850 °C for 5 h under open circuit conditions (d), and the fresh cell LSSM|ScSZ|LSSM (e), after the operation with pure CO at 900 °C for 5 h under open circuit conditions (f).

3.4. Performance degradation

For practical application, high operational stability is a prerequisite for fuel cells. For many SOFC systems operating on hydrocarbon fuel, carbon deposition over the anode may block the active sites and result in fast cell performance degradation [13]. Previously, we have demonstrated significant carbon deposition occurring over Ni-SDC and Ni-ScSZ anodes when they were exposed to CO atmosphere. To investigate the operational stability of the anodes on CO fuel in real fuel cell conditions, the fuel cells with the various anode materials were first tested by applying 3% water humidified H_2 as the fuel for 30 min, following which, the fuel was changed to CO, and the fuel cell was kept under OCV conditions with periodical *I–V* polarization measurement to obtain information of their power output at various periods. After operating for 180 min on CO fuel, the fuel gas was switched back to hydrogen, and the cells were polarized under a constant current density of 500 mA cm^{-2} (or 200 mA cm^{-2} for the cell with LSSM anode) for about half-hour

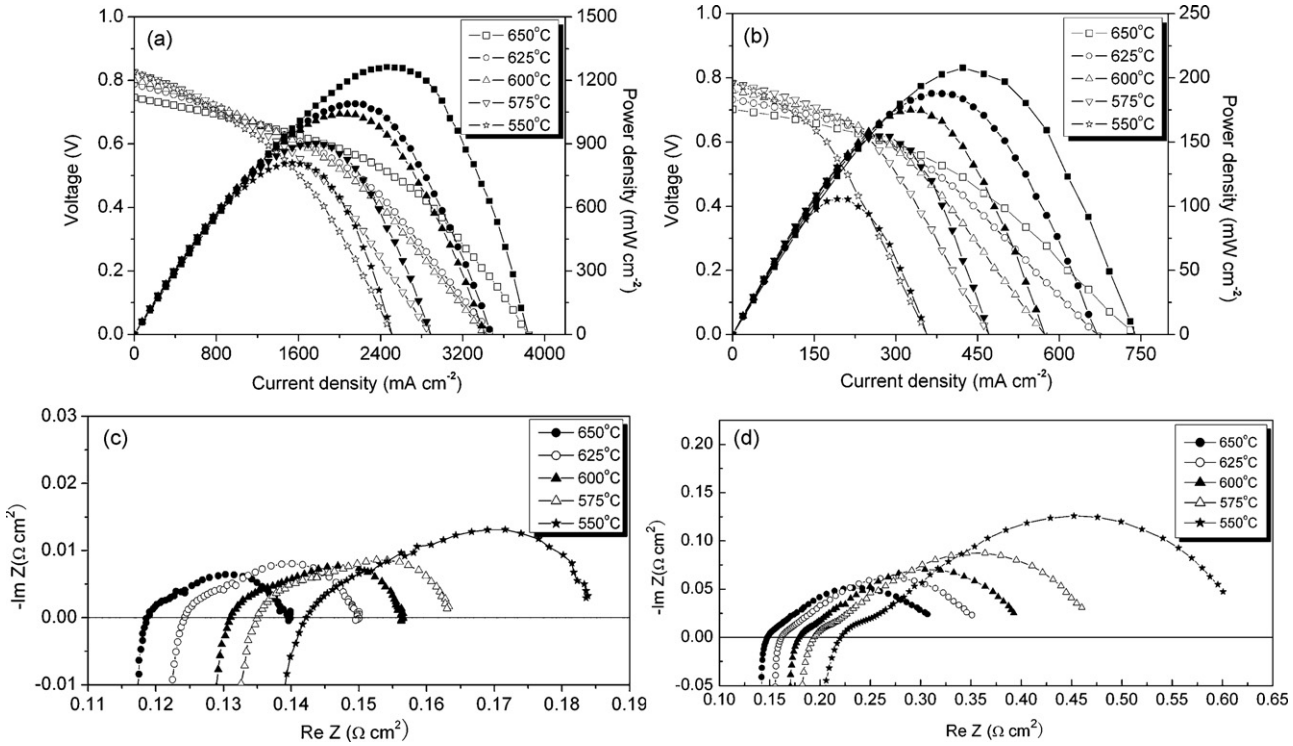

Fig. 8. The *I–V*, *I–P* curves and impedance spectra of the cell Ni-SDC|SDC|BSCF operating on hydrogen (a and c) and CO (b and d) at different temperatures.

to eliminate any carbon deposited over the anode. The cell performance under hydrogen fuel was periodically measured.

Fig. 11 shows the operating time dependence of the PPDs for the three fuel cells. For the cell of Ni-SDC|SDC|BSCF, the PPD obviously decreased with operating time, being 194 mW cm^{-2} at the initial stage, 176 mW cm^{-2} after 10 min, and only 104 mW cm^{-2} after 3 h operating on CO. The performance degradation of the cells with the Ni-SDC anode can be well explained by the coke formation over

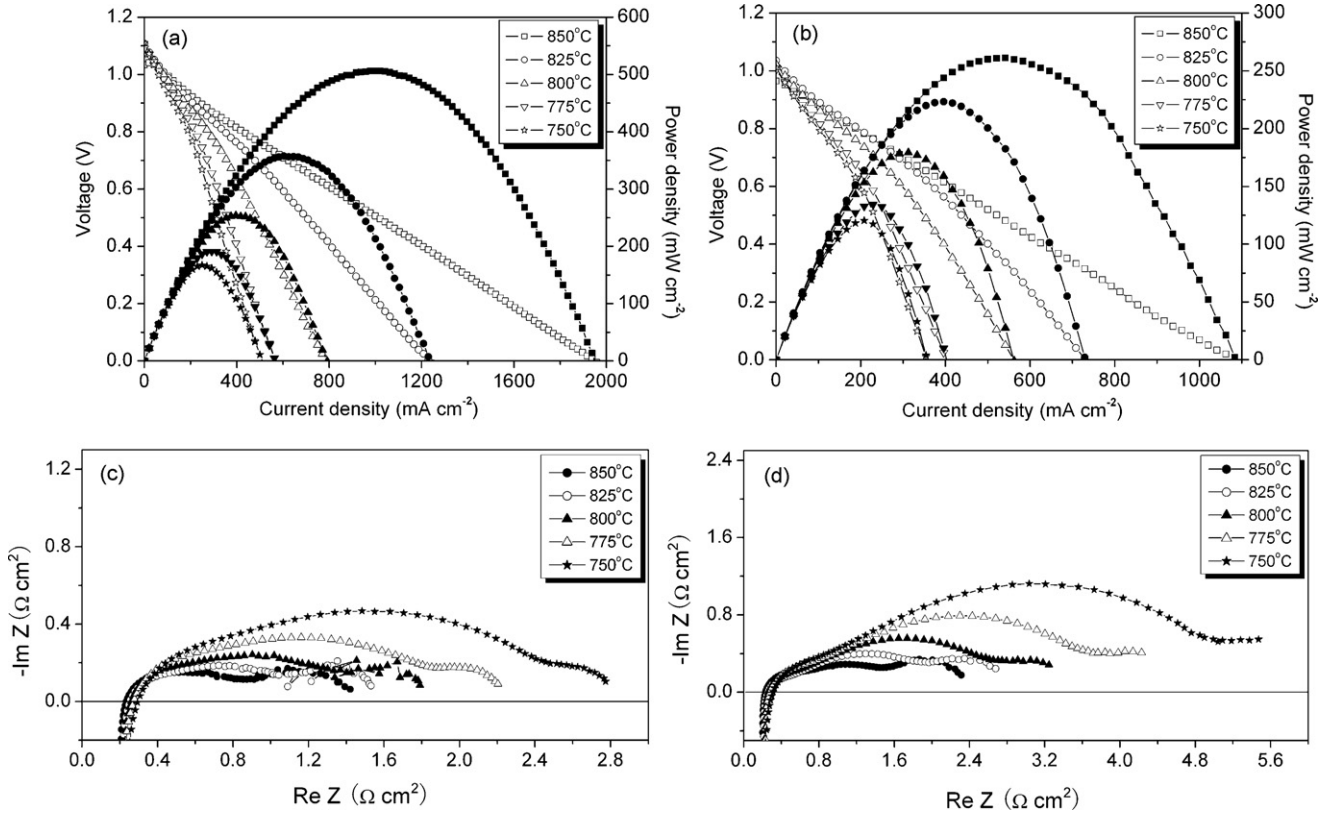

Fig. 9. The *I–V*, *I–P* curves and impedance spectra of the cell Ni-ScSZ|ScSZ|LSM operating on hydrogen (a and c) and CO (b and d) at different temperatures.

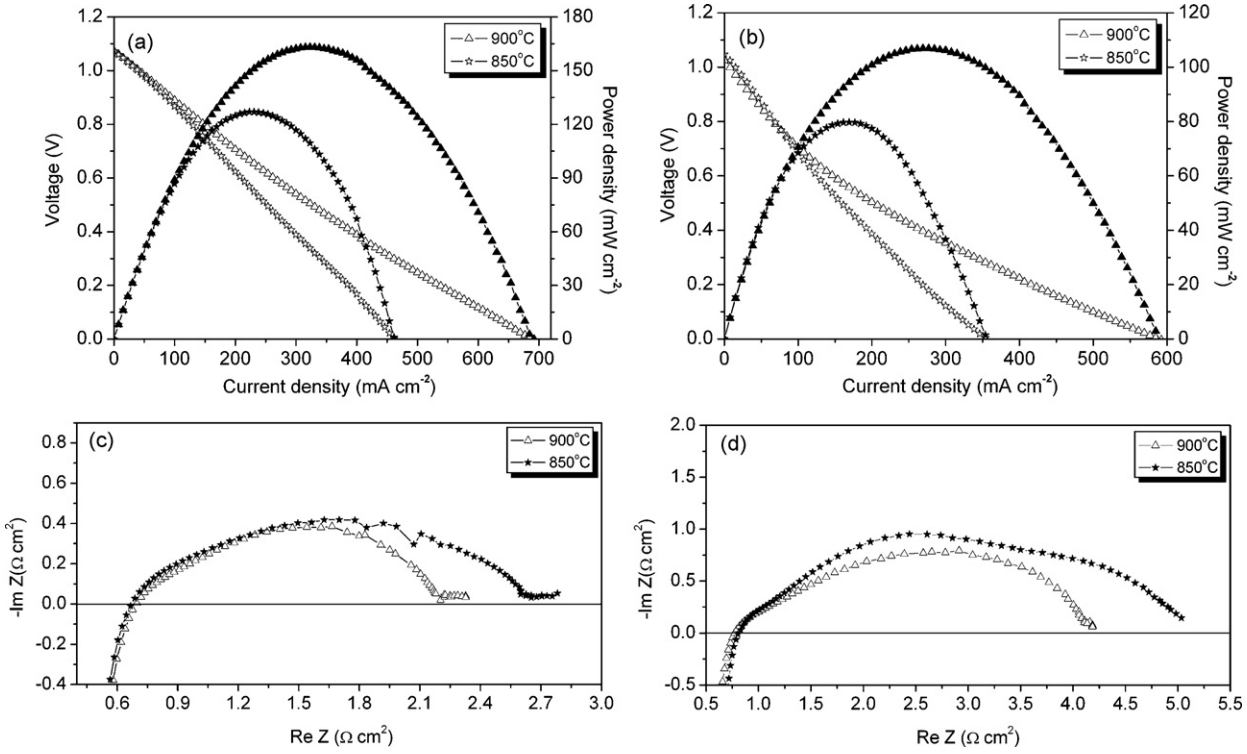

Fig. 10. The *I–V* and *I–P* curves and impedance spectra of the cell LSSM|ScSZ|LSSM operating on hydrogen (a and c) and CO (b and d) at different temperatures.

the anode surfaces, which may cover the active sites and result in a reduced triple phase boundary length for CO oxidation. The elimination of deposited carbon by polarization under hydrogen fuel did not result in restoration of cell performance. After the carbon elimination, the PPD was still only ~320 mW cm^{-2}. This suggests that the cell deterioration is irreversible. Similar observation was reported by Offer and Brandon [11]. In connection with the SEM results, it is likely that the sizeable carbon deposition pulverized the anode and significantly destroyed the anode microstructure.

For the cell of Ni-ScSZ|ScSZ|LSM, although its operating temperature was much higher than Ni-SDC|SDC|BSCF (850 °C versus 600 °C), the cell performance degradation rate was relatively slower. The PPD was 289 and 163 mW cm^{-2} for the initial value and after operation on CO for 3 h, respectively. The reduction in PPD is 43.6%, as compared with 46.4% for the cell Ni-SDC|SDC|BSCF. The smaller cell degradation rate could be attributed to a lower coke formation rate over the Ni-ScSZ anode than over the Ni-SDC anode. The cell performance was found to be largely recovered when the fuel was switched back to hydrogen.

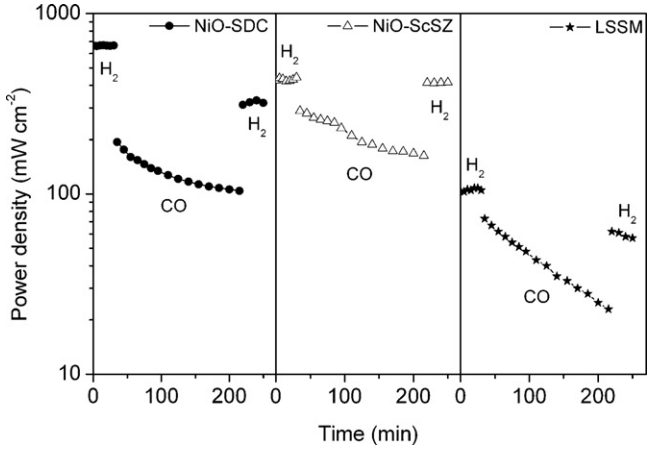

Fig. 11. The operation time dependence of the peak power density for the three fuel cells.

It was surprising to find that the performance degradation rate is the fastest for the cell LSSM|ScSZ|LSSM among the three cells. The PPD decreased from an initial value of 73 mW cm^{-2} to only 23 mW cm^{-2} after 3 h of operating on CO fuel at 850 °C. After the 3 h operation on CO fuel, the PPD retained only 31.5% of the initial value. Since there was almost no coke formed over the LSSM anode, as demonstrated previously, such degradation could not be explained based on the carbon deposition over the anode. For the perovskite anode, phase stability is a major concern, since the oxygen partial pressure of the anode atmosphere could be very low. Overly low oxygen partial pressure in the anode atmosphere may induce phase reduction and destroy the perovskite structure. To demonstrate the phase stability of the LSSM anode in CO atmosphere, LSSM powder was treated with various CO–CO_2 mixed gases at 850 °C for 3 h and then submitted for phase examination. Shown in Fig. 12 are the XRD patterns of the LSSM oxides after the treatment. They show that additional diffraction peaks appeared after the treatment in pure CO atmosphere, although the main perovskite phase was sustained. This suggests that LSSM is not sufficiently stable to withstand the highly reducing pure CO atmosphere, which results in the fast cell performance degradation with time operating on CO fuel. Previously, we have reported that LSSM was stable in humidified H_2 atmosphere, in which the calculated P_{O_2} is around 10^{-18} atm. For pure CO, P_{O_2} can be as low as 10^{-22} atm; such a low oxygen partial pressure then led to the partial reduction of LSSM and decreased its activity for the electro-oxidation of CO. Therefore, LSSM cannot be operated on dry CO. However, once some CO_2 was introduced into the CO fuel gas or the fuel cell was operated under current polarization, the oxygen partial pressure of the anode would increase substantially. The equilibrium oxygen partial pressure for CO–CO_2 mixed gases with 67.69%, 86.88%, and 39.85% CO_2 reaches 10^{-18}, 10^{-17}, and 10^{-19} atm, respectively. As shown in Fig. 12, by introducing the proper amount of CO_2 into the CO fuel gas, the LSSM phase

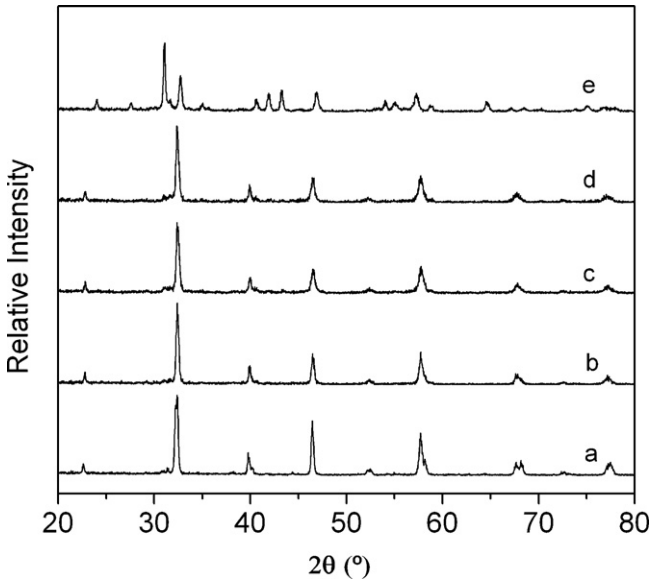

Fig. 12. XRD patterns of LSSM after various treatments: fresh sample (a), after the treatment CO–CO_2 mixed gases with 86.88% CO_2 (b), 67.69% CO_2 (c), 39.85% CO_2 (d), and pure CO (e).

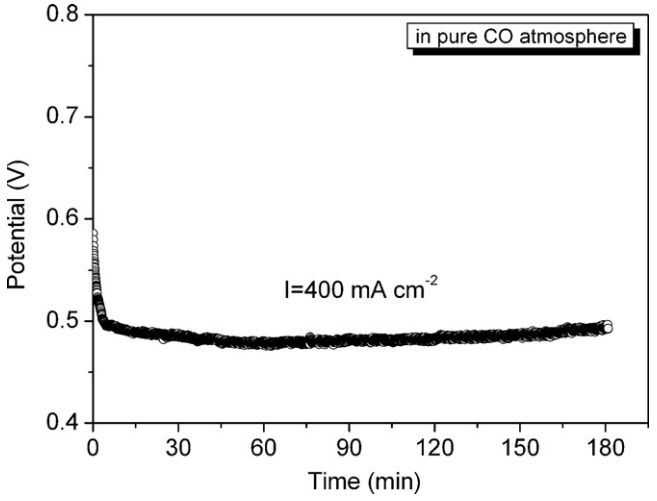

Fig. 13. Time dependence of the polarization curve of the LSSM electrode under a constant anodic polarization current of 400 mA cm^{-2} at 850 °C.

structure was stabilized. A stable cell performance could then be expected. On the other hand, the anode polarization results in the oxygen partial pressure over the anode surface to be considerably higher than in the fuel gas, allowing it to protect the anode from reduction. A stable cell performance could then also be expected. To support such an assumption, the performance stability of LSSM under polarization was tested. To eliminate the effect of the cathode, a three-electrode configuration was adopted. Shown in Fig. 13 is the polarization curve of the LSSM electrode under a constant anodic polarization current of 400 mA cm^{-2} in CO atmosphere at 850 °C for a period of 3 h. During the operation, the electrode performance was indeed fairly stable.

4. Conclusions

When applying CO as a fuel for SOFCs, coke formation over the anodes is a big concern because the Boudouard reaction is favored at the operating temperatures of SOFCs. The kinetics played a more important role than thermodynamics in the carbon deposition over the Ni-SDC and Ni-ScSZ cermet anodes. Higher operating temperature led to greater coke formation. The coke formed much more easily for Ni-SDC than for Ni-ScSZ cermet. The strong interaction between NiO and ScSZ ceramic component suppressed the coke formation over the Ni-ScSZ anode, while there was almost no such interaction between NiO and SDC in the Ni-SDC anode. The significant coke formation under OCV conditions led to damage of the anode microstructure by pulverization of the Ni-SDC anode and resulted in irreversible cell degradation when operating on CO fuel. For the Ni-ScSZ anode, the cell degradation was largely reversible. The LSSM anode was not structurally stable under a dry CO atmosphere, which resulted in rapid cell performance degradation under OCV conditions when operating on pure CO fuel. However, under current polarization, the cell with an LSSM anode can be stably operated on CO fuel. Ni-ScSZ and LSSM are superior to Ni-SDC as anodes for operating on CO fuel. The compositional modification is needed to successfully operate the Ni-SDC anode on CO-containing fuels.

Acknowledgements

This work was supported by the National Natural Science Foundation of China under Contract Nos. 20676061 and 20703024, by the National 863 Program under Contract No. 2007AA05Z133, and by the National Basic Research Program of China under Contract No. 2007CB209704.

References

[1] N.Q. Minh, J. Am. Ceram. Soc. 76 (1993) 563–588.
[2] R.J. Bellows, E.P. Marucchi-Soos, D.T. Buckley, Ind. Eng. Chem. Res. 35 (1996) 1235–1242.
[3] M. Krumpelt, T.R. Krause, J.D. Carter, J.P. Kopasz, S. Ahmed, Catal. Today 77 (2002) 3–16.
[4] E.D. Park, D. Lee, H.C. Lee, Catal. Today 139 (2009) 280–290.
[5] B.C.H. Steele, A. Heinzel, Nature 414 (2001) 345–352.
[6] A. Atkinson, S.A. Barnett, R.J. Gorte, J.T.S. Irvine, A.J. McEvoy, M. Mogensen, S.C. Singhal, J. Vohs, Nat. Mater. 3 (2004) 17–27.
[7] Y.B. Lin, Z.L. Zhan, J. Liu, S.A. Barnett, Solid State Ionics 176 (2005) 1827–1835.
[8] T. Hibino, A. Hashimoto, K. Asano, M. Yano, M. Suzuki, M. Sano, Electrochem. Solid-State Lett. 5 (2002) A242–A244.
[9] A. Wojcik, H. Middleton, I. Damopoulos, J.V. Herle, J. Power Sources 118 (2003) 342–348.
[10] M. Cimenti, J.M. Hill, J. Power Sources 186 (2009) 377–384.
[11] G.J. Offer, N.P. Brandon, Chem. Eng. Sci. 64 (2009) 2291–2300.
[12] S. McIntosh, R.J. Gorte, Chem. Rev. 104 (2004) 4845–4865.
[13] S. Park, J.M. Vohs, R.J. Gorte, Nature 404 (2000) 265–267.
[14] E. Perry Murray, T. Tsai, S.A. Barnett, Nature 400 (1999) 649–651.
[15] A.L. Lee, R.F. Zabransky, Ind. Eng. Chem. Res. 29 (1990) 766–773.
[16] W. Sangtongkitcharoen, S. Assabumrungrat, V. Pavarajarn, N. Laosiripojana, P. Praserthdam, J. Power Sources 142 (2005) 75–80.
[17] G. Goula, V. Kiousis, L. Nalbandian, I.V. Yentekakis, Solid State Ionics 177 (2006) 2119–2123.
[18] W.L.S. Faria, L.C. Dieguez, M. Schmal, Appl. Catal. B 85 (2008) 77–85.
[19] T. Iida, M. Kawano, T. Matsui, R. Kikuchi, K. Eguchi, J. Electrochem. Soc. 154 (2007) B234–B241.
[20] S.L. Jain, J.B. Lakeman, K.D. Pointon, J.T.S. Irvine, J. Fuel Cell Sci. Technol. 4 (2007) 280–282.
[21] S.W. Li, A.C. Lee, R.E. Mitchell, T.M. Gür, Solid State Ionics 179 (2008) 1549–1552.
[22] A.C. Lee, S.W. Li, R.E. Mitchell, T.M. Gür, Electrochem. Solid-State Lett. 11 (2008) B20–B23.
[23] Y.Z. Wu, C. Su, C.M. Zhang, R. Ran, Z.P. Shao, Electrochem. Commun. 11 (2009) 1265–1268.
[24] T. Hibino, A. Hashimoto, T. Inoue, J. Tokuno, S. Yoshida, M. Sano, Science 288 (2000) 2031–2033.
[25] M. Yano, A. Tomita, M. Sano, T. Hibino, Solid State Ionics 177 (2007) 3351–3359.
[26] Z.P. Shao, S.M. Haile, J. Ahn, P.D. Ronney, Z.L. Zhan, S.A. Barnett, Nature 435 (2005) 795–798.
[27] C.M. Zhang, Y. Zheng, R. Ran, Z.P. Shao, W.Q. Jin, N.P. Xu, J. Ahn, J. Power Sources 179 (2008) 640–648.
[28] T. Suzuki, P. Jasinski, V. Petrovsky, H.U. Anderson, F. Dogan, J. Electrochem. Soc. 151 (2004) A1473–A1476.
[29] N. Yoshida, T. Yamamoto, F. Minoguchi, S. Kishimoto, Catal. Lett. 23 (1994) 237–243.
[30] Y. Matsuzaki, I. Yasuda, J. Electrochem. Soc. 147 (2000) 1630–1635.
[31] A.M. Sukeshini, B. Habibzadeh, B.P. Becker, C.A. Stoltz, B.W. Eichhorn, G.S. Jackson, J. Electrochem. Soc. 153 (2006) A705–A715.

[32] K. Sasaki, Y. Hori, R. Kikuchi, K. Eguchi, A. Ueno, H. Takeuchi, M. Aizawa, K. Tsujimoto, H. Tajiri, H. Nishikawa, Y. Uchida, J. Electrochem. Soc. 149 (2002) A227–A233.
[33] P. Holtappels, L.G.J. De Haart, U. Stimming, I.C. Vinke, M. Mogensen, J. Appl. Electrochem. 29 (1999) 561–568.
[34] A. Weber, B. Sauer, A.C. Müller, D. Herbstritt, E. Ivers-Tiffée, Solid State Ionics 152–153 (2002) 543–550.
[35] G.O. Lauvstad, R. Tunold, S. Sunde, J. Electrochem. Soc. 149 (2002) E497–E505.
[36] O. Costa-Nunes, R.J. Gorte, J.M. Vohs, J. Power Sources 141 (2005) 241–249.
[37] H.X. Gu, R. Ran, W. Zhou, Z.P. Shao, J. Power Sources 172 (2007) 704–712.
[38] Y. Zheng, C.M. Zhang, R. Ran, R. Cai, Z.P. Shao, D. Farrusseng, Acta Mater. 57 (2009) 1165–1175.
[39] S. Takenaka, H. Umebayashi, E. Tanabe, H. Matsune, M. Kishida, J. Catal. 245 (2007) 392–400.
[40] S.W. Tao, J.T.S. Irvine, Nat. Mater. 2 (2003) 320–323.
[41] Y.H. Huang, R.I. Dass, Z.L. Xing, J.B. Goodenough, Science 312 (2006) 254–257.
[42] A. Yoshida, Y. Kaburagi, Y. Hishiyama, Carbon 44 (2006) 2330–2356.
[43] A. Cuesta, P. Dhamelincourt, J. Laureyns, A. Martinez-Alonso, J.M.D. Tascon, Carbon 32 (1994) 1523–1532.
[44] P. Lespade, A. Marchand, M. Couzi, F. Cruege, Carbon 22 (1984) 375–385.
[45] Z.P. Shao, S.M. Haile, Nature 431 (2004) 170–173.
[46] Q.L. Liu, K.A. Khor, S.H. Chan, J. Power Sources 161 (2006) 123–128.
[47] W. Zhou, R. Ran, Z.P. Shao, H.X. Gu, W.Q. Jin, N.P. Xu, J. Power Sources 174 (2007) 237–245.
[48] H.X. Gu, Y. Zheng, R. Ran, Z.P. Shao, W.Q. Jin, N.P. Xu, J. Ahn, J. Power Sources 183 (2008) 471–478.